FACULTY OF SCIENCE
UNIVERSITY OF COPENHAGEN

Spin waves and Quantum Phase Transitions in the near 1D Ising system $CoCl_2 \cdot D_2O$

Bachelor Project

Ane Kristine Baden & Sigrid Skovbo Adsersen

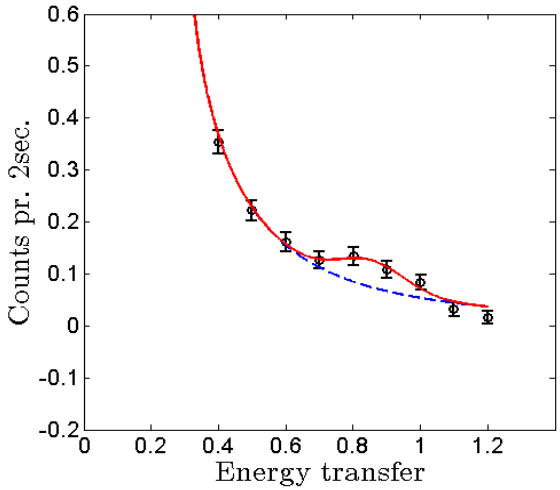

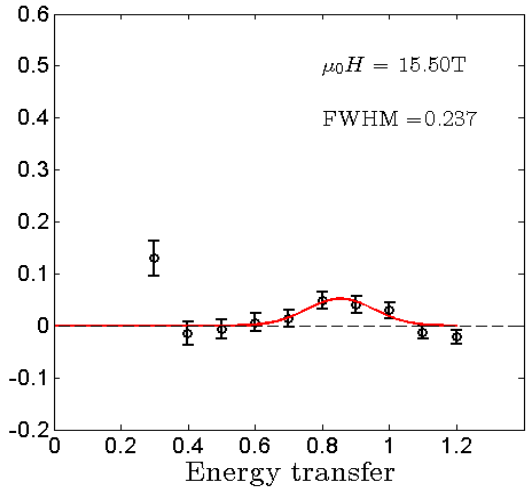

06 / 11 – 2013

Supervisor: Kim Lefmann

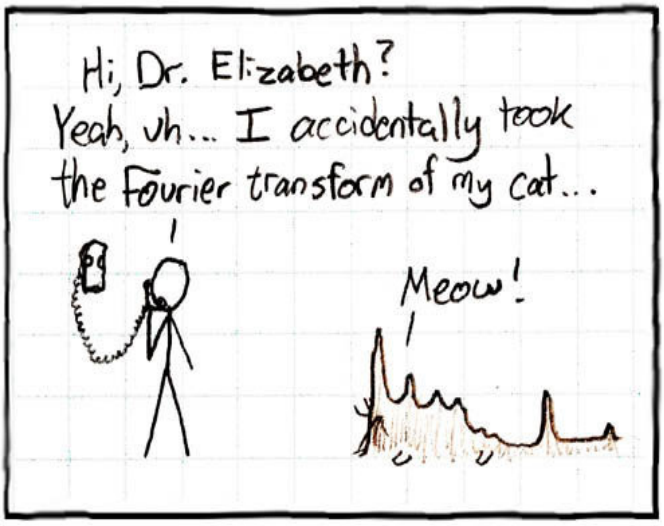
Hi, Dr. Elizabeth?
Yeah, uh... I accidentally took the Fourier transform of my cat...
Meow!

Contents

Abstract

In this project we have studied quantum phase transitions and spin waves as well as the magnetic ordering temperature for the $CoCl_2 \cdot 2D_2O$ crystal using neutron scattering and susceptibility measurements, respectively. The crystal is chosen for its Ising like behaviour. We used the FLEXX instrument at BENSC to measure spin waves and the quantum critical point. We found the critical field to be 16.10 ± 0.10 T, in good agreement with the value known from susceptibility measurements.
We tried to determine the ordering temperature by fabricating an AC-Susceptometer. We did observe some signal deviation at the expected temperature, 17.5 K, but due to noise and unexpected background behaviour, the whole experimental setup requires improvements before this result is reliable.
We finish of by evaluating the issues faced, assess the results and give our take on future improvements regarding both experiments.

Resume

I dette projekt har vi ved hjælp af hhv. neutronspredning og susceptibilitetsmålinger undersøgt spinbølger og kvantefase overgange samt ordningstemperaturen for krystallet $CoCl_2 \cdot 2D_2O$. Dette krystal er valgt pga. dens Ising lignende egenskaber.
Vi har i Berlin ved BENSC målt det kvante kritiske punkt til 16.10 ± 0.10 T med instrumentet FLEXX i god overensstemmelse med det kritiske felt bestemt ved susceptibilitetsmålinger.
Vi har forsøgt at bestemme ordningstemperaturen ved at fremstille et AC susceptometer. Vi observered nogle anormaliter ved den forventede ordingstemperatur, 17.5 K men grundet støj og uventede baggrundssignal kræver opstillingen flere forbedringer før resultatet er troværdigt.
Vi slutter opgaven af med evaluering af problemerne, vurdering af resultaterne samt et bud på mulige forbedringer ved begge forsøg.

Acknowledgements

We would like to thank the whole $CoCl_2 \cdot 2D_2O$ crew in the Neutron Scattering Group at HCØ. Firstly, our supervisor Kim Lefmann for giving us the exciting opportunity to explore the fascinating world of neutron scattering and all the benefits from it. Jacob Larsen for all his guidance towards understanding the $CoCl_2 \cdot 2D_2O$ crystal and all the (pleasant) hours of teaching and experimenting in Berlin. Ursula Bengaard for her endless patience regarding coilwinding and failing experiments in the basement at HCØ and Turi Kirstine Schäffer for providing crystals. Lastly we would like to thank all the technicians at NBI for the usage of their facilities and Per Hedegaard for providing bee wax.

1 Introduction

If you were to ask a non physicist (or maybe a non chemist) what a crystal is, most people would probably think of diamonds, snow flakes or maybe even salt. But truth is that most condensed matter in our everyday life, such as metals, are actually crystals! Depending on the structure of the lattice that spans the crystal it may possess a great variety of properties.
In this project we will focus on the magnetic properties of the crystal $CoCl_2 \cdot 2D_2O$, which is a monoclinic crystal with features that behave as a 1D Ising model below a certain ordering temperature. This behaviour gives us the opportunity to study a Quantum Phase Transition (QPT) in the crystal. QPT happens at zero temperature, i.e. there are no thermal fluctuations. To investigate the QPT we used magnetic neutron scattering and Triple Axis Spectroscopy and to investigate the ordering temperature we used an AC susceptometer.
Another quantum phase transition is found in the chemical doping of high temperature superconductors. Some materials experience superconductivity at very low temperatures, the goal is to chemically dope these materials to show the same behaviour at high temperatures, i.e. increase the ordering temperature of the compound, which the modern society can benefit greatly from since superconductors can lead current without any resistance. The principle of chemical doping is equivalent to a phase transition, e.g. a greater understanding of phase transitions will lead the way to a greater understanding of how to produce high temperature superconductors.

In this project we will introduce and explain the theory behind QPT as well as the experiments and experimental techniques used to observe the intriguing mechanism.

2 Magnetism

In this section we will explain the basics of magnetism, what a phase transition is and which quantum mechanical effects that describe our sample, the $CoCl_2 \cdot 2D_2O$ crystal.

2.1 Magnetism and Spin waves

All magnetic phenomena arise from an electric charge in motion. Suppose we have a planar closed loop which carries an electric current. The electric current will create a magnetic moment $\boldsymbol{\mu}$ which is perpendicular to the loop. In atoms the current loop originates from the electron orbiting the nuclei. The atoms magnetic moment lie along the same direction as the angular momentum $\mathbf{L}$ and they are proportional to each other by a γ factor called the gyromagnetic ratio. The magnetic moment is given in units of the Bohr magneton, μ_B.

The electron itself possesses a magnetic moment, which is known as the spin angular momentum, $\hat{\mathbf{S}}$. The sum of the orbital angular momentum and the spin angular momentum gives the total angular momentum $\mathbf{J}$. The combination of the angular momenta leads to the ground state configuration for the ion and can be found by using Hund's rules [3].

A magnetic solid consist of a large number of atoms with magnetic moments. The magnetic moment per unit volume defines the magnetization $\mathbf{M}$ of the solid.

Above a certain transition temperature the magnetic moments in a magnetic material will point in random directions giving a zero net magnetization. The material is thereby thermally disordered and is known as a paramagnet. If we cool below the transition temperature, the magnetic moments arrange themselves in a certain magnetic order. If the spins are aligned in the same direction, giving a non-zero net magnetization, the state will be ferromagnetic. If the spins are aligned opposite of its neighbors it is an antiferromagnetic state. See figure 1.

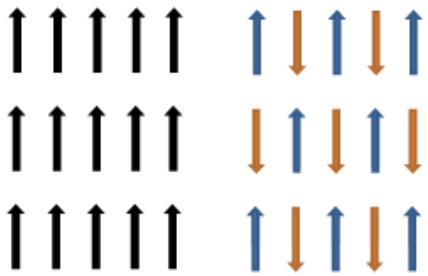

Figure 1: *The structure for a ferromagnetic (left) and a antiferromagnetic (right). The arrows indicates the direction of the spin*

The transition temperature at which a paramagnetic material becomes ferromagnetic is known as the *Curie Temperature* T_C, and for antiferromagnets it is the *Néel Temperature* T_N.
In a crystal the magnetic moments are fixed in a lattice. The interaction between these moments is the cause of magnetic order. A model that describes this interaction, is the Heisenberg model, given by the Hamiltonian,

$$\hat{H} = -\frac{J}{2}\sum_{i,j}\mathbf{S}_i \cdot \mathbf{S}_j, \tag{2.1}$$

where J is the exchange constant between the i'th and the j'th spin. For a ferromagnet $J > 0$ and for a antiferromagnet, $J < 0$, because all the magnetic moments sum to zero even in presence of an applied magnetic field.
The Heisenberg Hamiltonian arises from the Coulomb interaction and the Pauli principle [3]. In a ferromagnet the spins point along the same direction. If we flip one spin at the j'th site we get the state $|j\rangle = S_j^- |0\rangle$ where S_j^- is a lowering operator. When applying the Hamiltonian on state $|j\rangle$ we get, [3]:

$$\hat{H}|j\rangle = 2\left[(-NS^2J + 2SJ)|j\rangle - SJ|j+1\rangle - SJ|J-1\rangle\right]. \tag{2.2}$$

By diagonalize this Hamiltonian, we find a solution $|k\rangle$:

$$|k\rangle = \frac{1}{\sqrt{N}}\sum_j \exp(ikr_j)|j\rangle, \tag{2.3}$$

where N is the number of sites. $|j\rangle$ describes a flipped spin smeared out across the chain, creating a magnetic excitation known as a spin wave. This leads to the dispersion relation [3]:

$$\epsilon_k = 4JS(1 - \cos(ka)), \tag{2.4}$$

for the ferromagnetic spin waves where a is the lattice constant.

2.2 1D Ising Model

In a system where the spins are mainly able to point along z-direction the Heisenberg model 2.1 reduces to the famous Ising model. The 1D Ising Hamiltonian is [3],

$$\hat{H} = -J \sum_i S_i^z S_{i+1}^z, \tag{2.5}$$

where i denotes the i'th place in the spin chain. In a crystal there will be intrachain interactions described by 2.5 and interaction to neighboring chains. If the interaction between the spin chains are weak we can assume each chain as an isolated system.

Consider a chain with periodic boundary conditions with N spins. With $J > 0$ the ground state is a ferromagnet. The ground state has energy $-NJ/4$ when $S_i^z = +1/2$ [3]. Now consider the state with one flipped spin, see figure 2. This costs an additional energy $E = J$ because we turn two favourable interaction into unfavourable ones. The calculation is shown in Appendix A. However, there is an entropy gain equal to $S = k_B \ln(N)$ because of the degeneracy of this state, i.e. the flipped spin can occupied any one of the N sites.

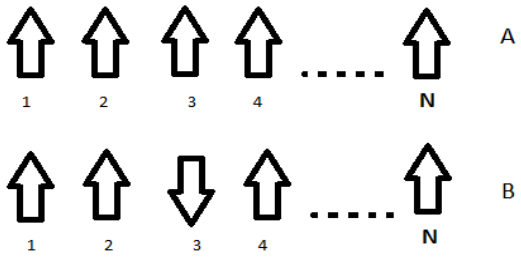

Figure 2: *The one-dimensional Ising model, (A) The ground state contains all N spins aligned ferromagnetically. (B) A single spin on site 3 is flipped. Adapted from [3].*

If the chain is very large ($N \to \infty$) the energy cost of a flipped spin remains the same but the entropy gain becomes infinite. The thermodynamical properties are determined from the free energy. At non-zero temperature, the entropy causes the free energy to go to $-\infty$. This means that a flipped spin can spontaneously flip and in fact no long range order occurs for $T > 0$. In conclusion, there is no thermally driven phase transition in Ising chains. We will return to this in section 2.4.

2.3 Ising Model in Transverse field

Consider applying an external magnetic field which is transverse to the spin direction. The Hamiltonian is [2],

$$\hat{H} = -J \sum_i S_i^z S_{i+1}^z - Jh \sum_i S_i^x. \tag{2.6}$$

The first term is the Ising Hamiltonian 2.5 and the second term is the Zeeman Hamiltonian. The constant h is the ratio between the Zeeman energy and the exchange energy constant J and is a dimensionless parameter, $h = g\mu_B B/J$.

The Ising term is dominant for weak magnetic fields. Assuming $h \to 0$ the Hamiltonian from eq. 2.6 is given by eq. 2.5, where the ground state is either $|0\rangle = |\downarrow\downarrow ... \downarrow\downarrow\rangle$ or $|\uparrow\uparrow ... \uparrow\uparrow\uparrow\rangle$. The ground state energy was found in section 2.2, $-NJ/4$. The lowest excitation is to flip half of the chain, so only one bond breaks. The energy cost of this is $JN/2$ [2].

In the strong fiels limit, $h \to \infty$, the Zeeman term in eq. 2.6 dominates and there is only one ground state, which is where all spins are aligned parallel or anti-parallel to the field, $|0\rangle = |\rightarrow\rightarrow ... \rightarrow\rightarrow\rangle$, where

$$|\rightarrow\rangle_i = -\frac{1}{\sqrt{2}}(|\uparrow\rangle_i + |\downarrow\rangle_i), \tag{2.7}$$

$$|\leftarrow\rangle_i = -\frac{1}{\sqrt{2}}(|\uparrow\rangle_i - |\downarrow\rangle_i), \tag{2.8}$$

Similar to the case in section 2.1 eq. 2.3 a magnetic excitation is described as a spin wave. From [11] the high field case is calculated, giving the exact solution to the dispersion relation for a flipped spin $|k\rangle$:

$$\epsilon_k = 2J(1 + h^2 + 2h\cos(k))^{1/2} \tag{2.9}$$

The change of ground state due to external magnetic fields is a fundamental property of the Quantum Phase Transition which we will explain in section 2.4.2.

2.4 Phase Transitions

2.4.1 Classical Phase Transition

The Classic Phase Transition (CPT), also called the thermal phase transition, describes a change in thermodynamic properties of a system. A typical example is the freezing of water: The transition between the fluid and solid state. Molecules in fluids have high symmetry, because they are in a state of complete translational and rotational symmetry. If we freeze the fluid the molecules form a lattice and the translational and rotational symmetry is broken [3].

The same physics applies to magnets. As mentioned, below T_C, a paramagnetic material orders into a ferromagnet. When the material is paramagnetic it has high symmetry, because it has complete rotational symmetry like in the fluid case. But if $T < T_C$, the magnetic moments will choose a certain direction and the rotational symmetry is broken (see figure 3). Notice that a symmetry cannot break gradually – either a particular symmetry is present or not.

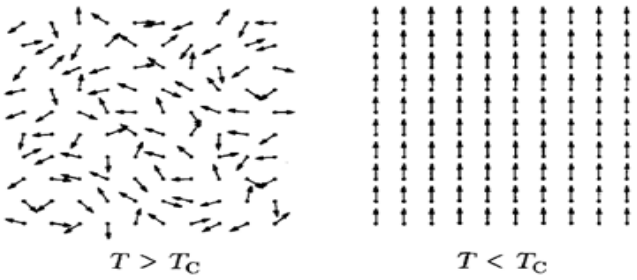

Figure 3: *Broken symmetry in magnets. Left shows a paramagnetic state with high symmetry. Right shows a ferromagnet with broken rotational symmetry [3].*

Associated to every phase transition is the concept of an order parameter. An order parameter is zero in a disordered state, and finite in an ordered state. For the ferromagnetic transition, the order parameter would represent the total magnetization of the system.

The CPT is driven by a competition between the internal energy of the system and the entropy of thermal fluctuations.
The free energy F is related to the internal energy U and the entropy S by $F = U - ST$. In order to minimize the free energy, at low temperature a system will choose the state with the lowest energy, i.e. the ground state. The ground state is usually ordered and will minimize U. As the temperature increases, the entropy S becomes more important and a disordered state is favored. This was shown in section 2.2, and as described in this section the existence of entropy generally prohibits CPT's in low dimensional systems.

2.4.2 Quantum Phase Transition

The Quantum Phase Transition (QPT) is a transition that happens at zero temperature where only quantum fluctuations are present [3]. The QPT is tuned by a non-thermal parameter like pressure or magnetic field.
Since asymmetry cannot change gradually, there will be a non-analytical point where the phase changes and the symmetry breaks. This point is denoted the Quantum Critical Point (QCP).
An example of a phase diagram is shown in figure 4. The QPT separates an ordered from a disordered phase. The region above the QCP is known as the quantum critical region. Not much is known about the quantum critical region and we will not elaborate it further in this project.

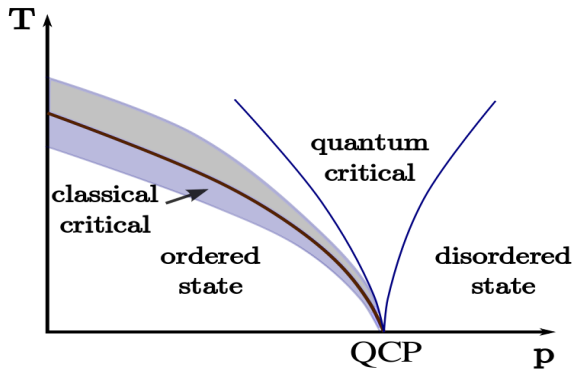

Figure 4: *Illustrates the classical- and quantum mechanical phase transition as a function of temperature T and a parameter p, which can be external magnetic field or pressure. For the 1D ising model the QPC seperates the Ising states from the Zeeman state.*

The system is disordered and purely classical at high temperatures. Around the classical phase transition, the system is governed by thermal fluctuations, shown in figure 4 as the light grey area. This region becomes narrower with decreasing temperature and converges towards the QCP.

In this project we will try to measure this QPT in the compound $CoCl_2 \cdot 2D_2O$, which has been reported as a good candidate for observing this phenomena [7]. But first we will discuss why cobalt chloride is a good candidate by looking into its magnetic properties.

3 Sample

In literature $CoCl_2 \cdot 2D_2O$ is considered as an Ising model [7]. We will go through the structural properties of the crystal and ellaborate the magnetic properties that make $CoCl_2 \cdot 2D_2O$ well suited for our project.

3.1 Structure

$CoCl_2 \cdot 2D_2O$ comes in large (a couple of centimetres long) needle shaped, purple crystals. The structure of $CoCl_2 \cdot 2D_2O$ has been investigated by B. Morosin and E. J. Graeber [9] and many others. For a general introduction to crystal structures, see Appendix B. The crystal structure is monoclinic [5], which means that two of the lattice angles are perpendicular, while the is angle greater than 90°, see figure 5. The monoclinic structure makes the orientation of the crystal challenging, see section 6.2.2. The crystal belong to the space group $C_{2/m}$, with the room temperature lattice constants, $a_1 = 7.256$ Å, $a_2 = 8.575$ Å, $a_3 = 3.554$ Å. $\beta = 97.60°$ [8].

The crystal structure consists of chains of Co^{2+} ions along the**c**-axis, separated from each other by Cl^-. Each Cl^- ion is shared by two Co^{2+} ions, figure 6.

In the crystal, the spins point along **b**. The interaction between the spin chains make the $CoCl_2 \cdot 2D_2O$ crystal magnetically interesting. This will be discussed in the following section.

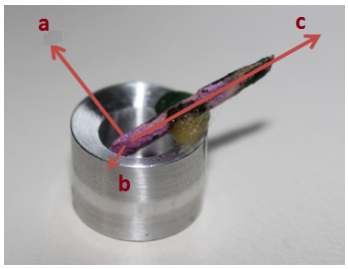

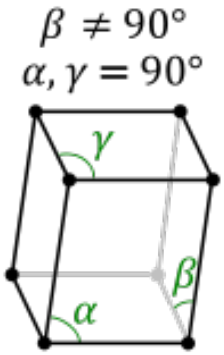

Figure 5: ***Left****: illustrates the actual crystal with its lattice vectors, where* **c** *is along the crystal,* **a** *is perpendicular to both* **c** *and* **b** *and* **b** *is pointing out of the paper plane.* ***Right*** *illustrates a monoclinic crystal.*

3.2 Magnetic Properties

The $CoCl_2{\cdot}2D_2O$ crystal is an antiferromagnetic structure in 3D but looking at the individual chains we get a 1D ferromagnetic structure in the **c** direction. Figure 6 shows the spin configuration in the crystal. Between the chains the interactions are antiferromagnetic and tend to order the spins of a ferromagnetic chain antiparallel to those of the neighboring chains. The interaction between the Co^{2+} spins within the same chain is much stronger than the interactions between chains, [7].

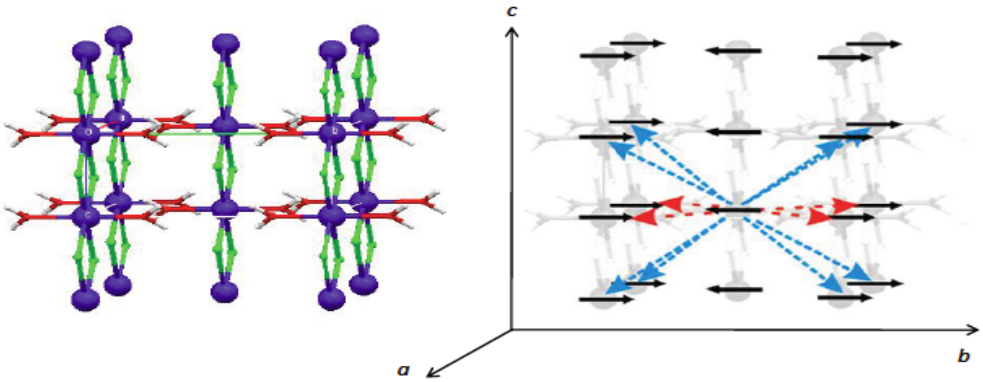

Figure 6: ***Left:*** *The structure of* $CoCl_2{\cdot}2D_2O$*. The blue color represents cobalt, the green chloride, the red oxygen and the white hydrogen.* ***Right:*** *The black arrows show the direction of the spins. The red arrows show the four interchain interactions in the plane of the spin. The blue arrows show the eight diagonal interchain interactions [14].*

Furthermore, the exchange interactions are anisotropic, with an easy **b** axis. It is because of this anisotropy that we are able to regard the individual spin chains in $CoCl_2{\cdot}2D_2O$ as Ising-like chains, where the spins are $|\uparrow\rangle$ or $|\downarrow\rangle$ with respect to the **b** axis, [7].

Neighboring chains are weakly bonded by the water molecules. The excitation spectra was measured by neutron scattering by W. Montfrooij who showed that the ferromangetic

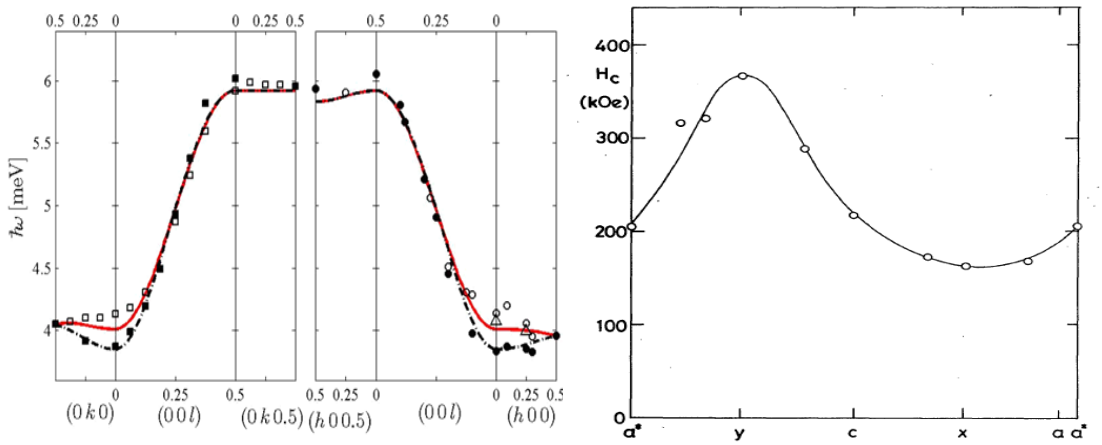

Figure 7: ***Left**: Measured spin-wave energy as a function of wave vector, q [15]. The dispersion is almost constant along h and k, but grows in the l - direction which indicates that $CoCl_2{\cdot}2D_2O$ is not a perfect 1D system in the* **c** *- direction, along the cobalt-chains. The dispersion in* **c** *is due to interaction between chains described by the Heisenberg Hamiltonian, eq. 2.1.* ***Right:** Susceptibility measured critical field in the (**a**,**c**)-plane. The minimum critical field is $H_c = 16.2 \pm 0.05$T [12].*

exchange constant in $CoCl_2{\cdot}2D_2O$ is about 5 times as big as the antiferromagnetic nearest neighbour interactions, [15]. In [15] the spin waves for $CoCl_2{\cdot}2D_2O$ in zero field is shown. The dispersion is almost constant along h and k, but disperse in the l - direction which indicates that $CoCl_2{\cdot}2D_2O$ is a 1D system in the **c** - direction, along the cobalt-chains, see figure 7. The dispersion in the l direction suggest a weak Heisenberg interaction (eq. 2.1), e.g. the Ising chain is not perfect.
A. Narath [10] and others have measured the phase transition of $CoCl_2{\cdot}\ 2D_2O$ at $T_c = 17.5$K, going from a paramagnetic phase above T_c to an the magnetically ordered state below T_c.

H. Mollymoto et al. [12] determined the critical field in a transverse field, H_c at which the QPT should occur, in the (**a**,**c**)-plane, to $H_c = 16.2 \pm 0.05$T.
Thereby we can conclude that $CoCl_2{\cdot}\ 2D_2O$ is an approximate physical realization of a 1D Ising system with a QPT below $T_c = 17.5$K and at approximately $H_c = 16.2$T. In this project we will investigate the magnetic properties for the $CoCl_2{\cdot}\ 2D_2O$ and identify the QCP.

4 Magnetic Neutron Scattering

4.1 Basics properties of the Neutron

The neutrons used in scattering experiments can be created in two ways: Through fission or the more modern technique, spallation. We used the triple axis instrument FLEXX at HZB, Berlin, where neutrons are produced by a fission reactor.

Neutron scattering has significant advantages over other experimental techniques, such as X-rays, in the study of magnetic structure and dynamics.

The neutron is an elementary particle and consists of three quarks (udd), it is electrically neutral but carries a magnetic moment. The lack of charge enables the neutron to penetrate the bulk of solid matter, but it can observe magnetic properties of the material. The magnetic moment of the neutron interacts with the spin of uncompensated electrons. The neutron magnetic moment is given by:

$$\boldsymbol{\mu} = \gamma \boldsymbol{\mu}_N \tag{4.1}$$

$\gamma = -1.913$ is the neutron magnetogyric ratio and the nuclear magneton $\boldsymbol{\mu}_N = 5.051 \cdot 10^{-27}$ J/T. Unlike protons that are stable, neutrons decay with a mean lifetime of $\tau = 886$ s, ideal for scattering experiments since the duration of the scattering mechanism is a fraction of a second [1].

Like all other particles, neutrons exhibit a particle wave duality. In neutron scattering experiments neutrons behave as particles when they are created and when they are detected. When impinging on the sample they behave as waves. This is explained further in section 4.2. The de Broglie wavelength of a particle moving at constant velocity v is defined as [3],

$$\lambda = \frac{2\pi\hbar}{mv} \tag{4.2}$$

This relation between wavelength and velocity makes it possible to tune the neutron wavelength to be comparable with the lattice spacing in the crystal used in the experiment. This is done by cooling the neutrons, and is described further in in section 4.3. The wave nature is also described in terms of the neutrons *wave number* $k = 2\pi/\lambda$ or a wave vector $\boldsymbol{k} = k \cdot \hat{\boldsymbol{k}}$.

4.2 Basics of Neutron Scattering

With the knowledge of basic crystallography (see Appendix B) and the neutron properties in mind, we now have the tools to describe the basics of neutron scattering. We will explain how a neutron is scattered from a crystal lattice, and introduce elastic and inelastic scattering.

Consider the situation where a neutron with a well-defined velocity is scattered by a single nucleus, which is somehow fixed in a certain position as shown in figure 8. When leaving

the nucleus, the scattered neutron is a spherical wave. In general the neutron scatter from more than one nucleus. The wave scattered from one nucleus will add to the wave scattered from another nucleus and so on creating interference. This interference is a central aspect in most scattering techniques [1].

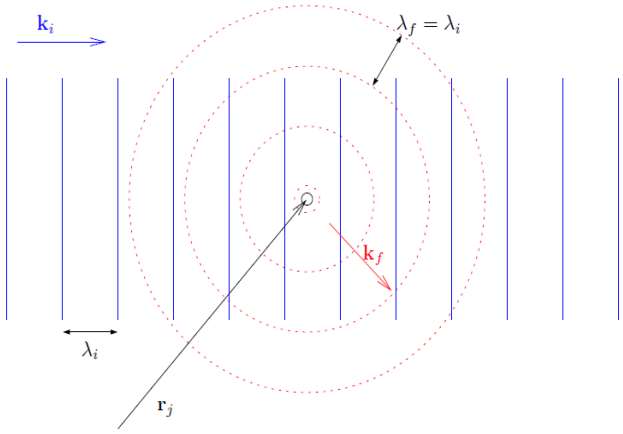

Figure 8: *A plane wave hitting a small target creating a spherical wave, [1].*

The difference between the incoming ($\mathbf{k}_i$) and outgoing ($\mathbf{k}_f$) wave vector is described as the scattering vector $\mathbf{q}$, defined as:

$$\mathbf{q} = \mathbf{k}_i - \mathbf{k}_f \tag{4.3}$$

This equation is the essence of scattering. The total phase of the scattered wave from a nucleus at the position $\mathbf{r}_j$ is then given by $A \cdot \exp(i\mathbf{q} \cdot \mathbf{r}_j)$, with A being a constant[1].

There are two kinds of neutron scattering: inelastic and elastic. In neutron scattering experiments elastic scattering is used to measure the crystal structure and inelastic scattering is used to measure the excitations. In the next two section the two types of scattering will be explained further.

4.2.1 Crystal Lattices, Diffraction and Elastic Scattering

An important feature of crystals is their ability to scatter for example x-rays or neutrons. To understand the scattering mechanism, we will introduce the scattering condition and derive Braggs law.

When describing a wave scattering off a target (for example a reflective surface such as glass or maybe an atom) we look at the wave vectors of the incoming and reflected beam, $\mathbf{k}_i$ and $\mathbf{k}_f$. These two vectors define the scattering vector $\Delta\mathbf{k} = \mathbf{k}_i$ - $\mathbf{k}_f = \mathbf{q}$, see fig. 9.

Scattering is described through the reciprocal space. Reciprocal space is the Fourier transform of real space, i.e. the real vectors $\mathbf{a}_1$, $\mathbf{a}_2$ and $\mathbf{a}_3$ will be replaced by the reciprocal lattice vectors $\mathbf{b}_1$, $\mathbf{b}_2$ and $\mathbf{b}_3$ (see Appendix B). These vectors span the reciprocal lattice. From these vectors we form a vector $\boldsymbol{\tau}$,

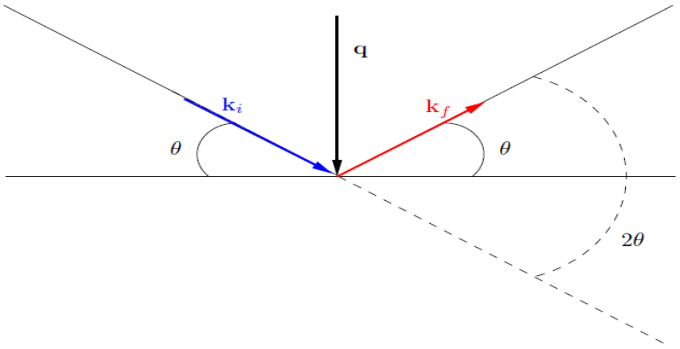

Figure 9: *A simple model of a neutron scattered from a sample. The incoming wave vector is $\boldsymbol{k}_i$, the outgoing wave vector is $\boldsymbol{k}_f$. They define the scattering vetcor $\boldsymbol{q}$ [1].*

$$\boldsymbol{\tau} = h\mathbf{b}_1 + k\mathbf{b}_2 + l\mathbf{b}_3. \tag{4.4}$$

(h, k, l) denote the lattice plane.

In order for a wave (both neutron- and X-rays) to scatter off a crystal it must hit a plane of atoms in the lattice, from the Laue Condition $\mathbf{q} = \boldsymbol{\tau}$ i.e. the scattering vector must be equal to a reciprocal lattice vector [5]. Thus we introduce a condition known as the diffraction condition for elastic scattering. Elastic scattering is a process where the kinetic energy of a particle is conserved. In this process a momentum transfer from the neutron to sample take place. This leads to a tiny recoil of the entire sample, but the internal state of the sample remains unchanged. Since the energy is conserved then $k_i = k_f = k$, see figure 9, which gives,

$$q = 2k\sin(\theta), \tag{4.5}$$

thus, we can derive Bragg's law for crystal diffraction:

$$2d\sin(\theta) = n\lambda \tag{4.6}$$

An important thing to note is the fact that scattering will only happen if λ is less than $2d$ and can only be distinguished if λ is not too small, which is why neutrons and X-rays are good candidates for crystal diffraction, since their wavelengths are of sizes comparable to the inner distances in the lattice.

The theory described above applies for most crystallography, but we are able use most of this theory in our experiment which concerns magnetic neutron scattering.

In a magnetic material a unit cell is formed, but instead of having atoms as the grid points, we will focus on the spin of the atoms, see figure 10. Depending on what kind of magnetic material the spin will allign themselves, as explained in section 2. When scattering off magnetic dipoles, magnetic excitations are possible and are detected as an energy differences between the initial neutron state with wave vector $\mathbf{k}_i$ and final state with wave

vector $\mathbf{k}_f$. This is called inelastic scattering and is explained further in section 4.2.2.

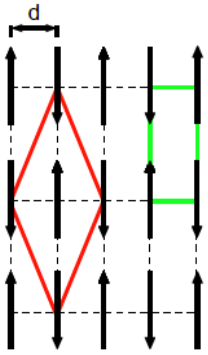

Figure 10: *An illustration of two types of magnetic unit cells in 2D. The red shows a antiferromagnetic unit cell, every spin is surounded by four neighbors of opposite spin. The green illustrates a ferromagnet and structural unit cell, [2].*

4.2.2 Inelastic Neutron Scattering

Inelastic scattering is a process in which the kinetic energy of a particle is not conserved, in contrast to elastic scattering. In this process, the neutron delivers energy to or absorbs energy from the scattering system. The energy transfer for a neutron is defined as,

$$\hbar\omega = E_i - E_f = \frac{\hbar^2(k_i^2 - k_f^2)}{2m_n} \tag{4.7}$$

Note that the energy and momentum change is defined with opposite sign of most definitions of changing properties, so that neutron energy loss gives a positive value of $\hbar\omega$.

Upon performing the experiment for this project we used both elastic and inelastic scattering. The instrument used for this is described in detail below.

4.3 Triple-Axis Spectroscopy

There are several different means of doing neutron scattering. One of these is to use Triple Axis Spectroscopy (TAS). This experimental method allows us to measure both elastic and inelastic scattering. When using TAS it is possible to fix initial parameters (such as energy or angle). The idea behind the TAS is relatively simple: by knowing the incoming energy of the neutron wave you make a scan of the scattering function in energy and momentum space. At some point a peak will appear (similar to a game of Battleships). The peak determines the amount of energy transfer or absorption in the sample. Depending on what kind of scattering is present (see section 4.2.1 or 4.2.2) the peak will reveal either structural information or excitations in the sample. In this experiment we used the triple axis spectrometer, FLEXX located at the Helmholtz center in Berlin (HZB).

The name triple axis spectrometer arises from the anatomy of the instrument which consists of the monochromator, the sample and the analyzer. The monochromator and the analyzer is most often made off the same materiale, in our case pyrolytic graphite. The

principle of the triple-axis neutron spectrometer is shown in figure 11.

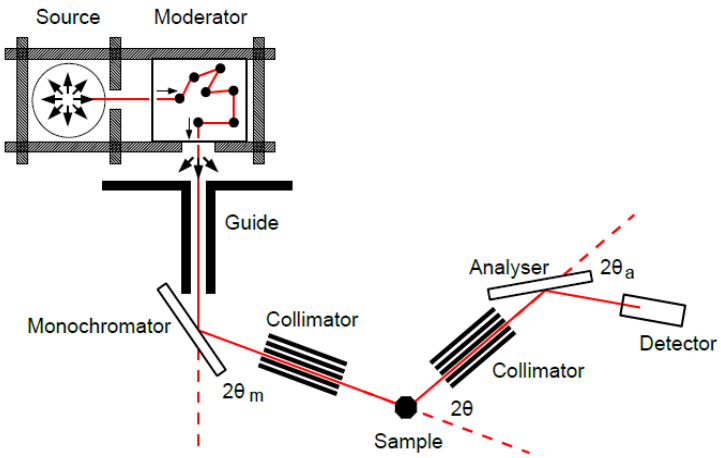

Figure 11: *The principle of the triple-axis neutron spectrometer. The three most important features are the monochromator, the sample and the analyzer, giving three axes [2].*

1. **Source**: Fission reactor. Produces neutrons with energies in the MeV range.
2. **Moderator**: Decreases the energies from MeV to meV by neutrons repeatedly colliding with a weakly absorbing material. In HZB a liquid hydrogen moderator at 25 K is used.
3. **Guide**: Transports the neutrons from the source to the monochromator to prevent high background contamination of the signal. If the experiment is performed too close to the source there will be high background contamination.
4. **Monochromator**: Selects neutrons with a well defined energy, due to Bragg's law, eq. 4.6. The incident energy depends on the monochromator material and its angle $2\theta_m$.
5. **Collimator**: Narrows the neutron beam in the desired direction.
6. **Sample**: Our sample under investigation. Scatters the neutrons. We are interested in those scattered by an angle 2θ
7. **Analyzer**: Selects the outgoing energy of the neutrons, due to Bragg's law, eq. 4.6. The outgoing energy depends on the analyzers material and its angle $2\theta_a$.
8. **Detector**: Measures the neutrons.

When the neutron beam has been moderated, it is guided towards the single crystal monochromator which, due to the Bragg reflection (eq. 4.6), selects neutrons of a particular energy. The monochromatic beam is then sent towards the sample by using a collimator. In our experiment the sample was placed in a 15 T cryomagnet where the field was increased with a Dy-Booster which added 2.5T to the field of the cryomagnet, giving

a maximum field of 17.5T, the highest continous field in any neutron scattering experiment, [2]. This gives us the opportunity to reach the QCP at 16.2T [12]. TAS is able to measure both inelastic and elastic neutron scattering because of the monochromator and the analyzer. If $2\theta_m = 2\theta_a$ then the energy is conserved and we measure elastic neutron scattering. If the energy of the diffracted beam is not consistent with the analyzer settings, the signal disappears. The final signal is detected in the detector as a count number.
We used TAS to measure magnetic structures and spin waves in the sample $CoCl_2 \cdot 2D_2O$, which has been reported as a good candidate for observing quantum phase transition [7].

In neutron scattering experiments it is important to know the ordering temperature for the given sample. At temperatures above the ordering temperature, the thermal interactions between the crystals spins dominates. Below, the thermal interactions are suppressed and quantum effects can be observed. The transition temperature for $CoCl_2 \cdot 2D_2O$ has been observed at 17.5 K, [10]. To measure the ordering temperature for $CoCl_2 \cdot 2D_2O$ we used an AC susceptometer and will be described in the following section.

5 AC Susceptibility

The AC susceptometer is able to measure the magnetic susceptibility as a function of frequency and temperature at weak magnetic fields. In the following sections we will describe the theoretical background, the experimental technique and how we convert the voltage measurements from `LabVIEW` to the magnetic susceptibility.

5.1 Susceptibility

Magnetic susceptibility is a dimensionless constant that indicates the degree of magnetization, M, of a material in response to an applied magnetic field, H:

$$\mathbf{M} = \chi \mathbf{H} \tag{5.1}$$

The susceptibility gives insight into the magnetic nature of the substance; the material is paramagnetic if the magnetic susceptibility is positive i.e. an induced magnetization is aligned parallel to an external magnetic field. If the susceptibility is negative such that an induced magnetization is aligned anti-parallel to the external magnetic field the material is diamagnetic.
In general most materials are non-linear, and we therefore change the definition so the magnetic susceptibility is a gradient of the magnetization with respect to the supplementary field,

$$\chi \equiv \frac{\partial \mathbf{M}}{\partial \mathbf{H}} \tag{5.2}$$

The susceptibility can be expressed as a function of temperature, [3],

$$\chi \propto \frac{1}{\mathrm{T} - \theta} \tag{5.3}$$

where θ is the Weiss temperature. If the substance i ferromagnetic θ=T_C, if the substance is antiferromagnetic θ=$-\mathrm{T}_N$.

The main concept of an AC susceptibility measurement is to induce an oscillating magnetic field into the sample by using coils. The response from the sample due to its magnetic properties is then picked up by a second inductive coil. We will now discuss this in further detail.

5.2 Design and Set-up

The susceptometer induces a varying magnetic field by sending AC current through two primary coils (D_1 and D_2). Inside the primary coils there are secondary coils (the pickup coils), see figure 12.

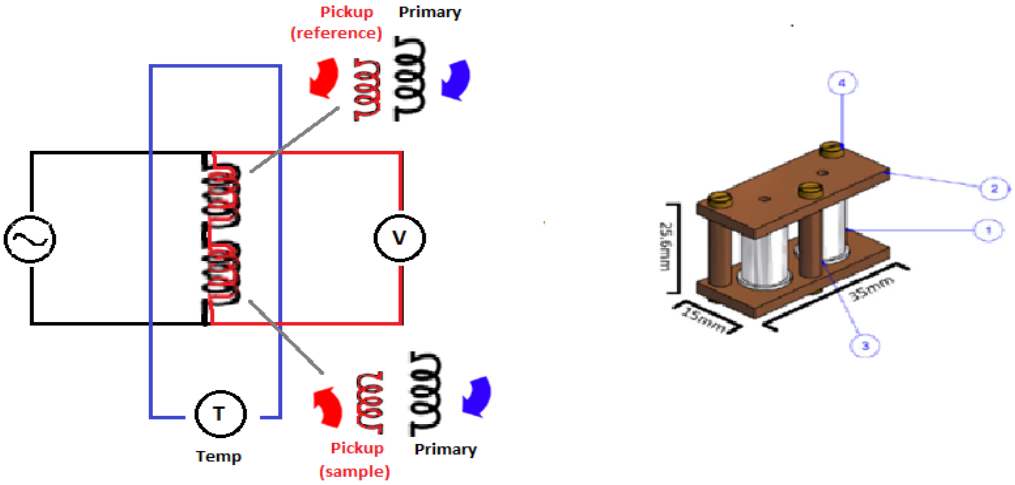

Figure 12: *The principle of the susceptometer.* ***Left****: A illustration of the setup for the susceptometer.* ***Right****: A illustration of the coil setup. (1) The primary coil. (2) Copperplates. (3) Metallic rod. (4) Brass screws. The coil setup was all build to handle low temperatures.*

The two pickup coils are wound in opposite directions and electrically connected in series. The sample is placed in one of the pickup coils (the sample coil) while the other pickup coil (the reference coil) is left empty.
The primary coils had approximately thrice as many windings as the pickup coils and were wound in the same direction so their magnetic fields were equally strong. Hence, the pickup coils cancel each other out. When applying the sample, the sample coil would give a change in the magnetic field and will not cancel out with the reference coils field. The number of windings and the size of the thread for each coil is noted in table 1.

	D1 and D2	P1	P2
Solenoid length [cm]	2	2	2
Solenoid diameter (outer) [cm]	1	0.7	0.7
Number of windings	390	928	895
Thread thickness [mm]	0.18	0.06	0.06

Table 1: *Table of the giving measures of our coils. D1, D2 are the Primary coils and P1, P2 are the Pickup coils.*

Note that the number of windings are different for the two pick up coils. The copper thread used to wound the coils were very thin and broke easily. After many re-woundings we reached a time limit, and we chose to stop making new coils and started measuring with the ones we had. The difference in number of windings gave us a difference in voltage between the two coils at around 0.33 mV. In the assembling we used D1P1 and D2P2 combined. The pickupcoils had an individual signal of 15.55mV (P1) and 15.13mV (P2). The coil set-up was mounted on the cooling finger of a Cryodyne CTI-Cryogenics Model 22 cryocooler which was supplied by a CTI-Cryogenics 8200 compressor with helium. To prevent thermal radiation from heating the sample, the cooling finger was shielded by a cylindrical shield wrapped in aluminium foil.
A Balzers-Pfeiffer vacuum pump reduced the pressure in the cooling chamber to approximately 0.03 mbar and it was measured by 300 series Convection Vacuum Gauge Module design by Kurt J. Lesker company.
The temperature of the susceptometer was measured with a LakeShore DRC-91C temperature controller connected to a diode. The voltage drop and the frequency were measured with a lock-in amplifier. An overview of the set-up is shown in figure 13.

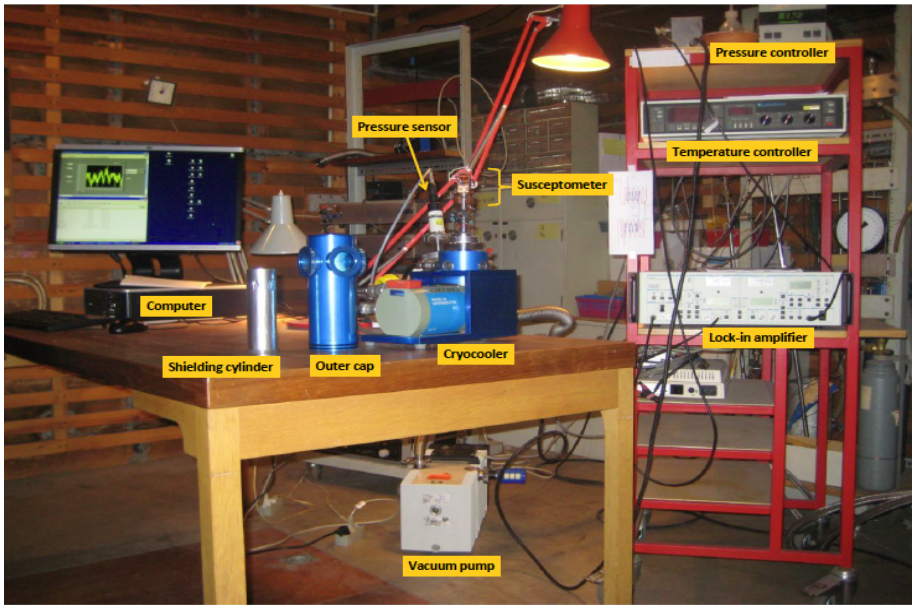

Figure 13: *The experimental setup. This picture was taken by Turi Kirstine Schäffer during her bachelor project [14] which is similar to ours except for the pressure controller which was replaced with the 300 series Convection Vacuum Gauge Module.*

LabVIEW was used to record the voltage difference between the sample and the reference coil from the lock-in amplifier. We could not connect the temperature controller correctly to LabView, this is discussed in 6.1.

6 Data

In this section we will analyze our measurements on $CoCl_2 \cdot 2D_2O$ from the different experiments. We will start by analyzing the crystals magnetization with the AC susceptometer and calculate its ordering temperature for which the quantum effects should appear. The neutron scattering experiment is used to find the QCP and investigate the spin waves in the crystal. All data was analyzed in MatLab and some was simulated in McStas, [19].

6.1 Susceptometer

Before performing the the actual susceptibility measurements we did a few tests to determine that the setup was working. This is listed in Appendix D.

The four coils were assembled as in figure 12 and placed it on the cooling finger of the cryocooler. The crystal sample was placed inside the sample coil, and fixed on a copper wire with bee wax to ensure thermal contact with the rest of the susceptometer. We did three independent measurements: one with just the bee wax and the copper wire to measure the background signal, one with a superconductor sample (Bi-2223) and finally we used $CoCl_2 \cdot 2D_2O$. The sample Bi-2223 was in small pieces at around 1-2 mm and the $CoCl_2{\cdot}2D_2O$ was one piece at around 2-3 cm.

Due to technical difficulties using the temperature controller we plugged the temperature manually into LabView in steps of $\sim$2K. To find the temperature for each time step, we plotted the temperature as function of time and interpolated to get a continuous temperature spectrum.
Combining the voltage measurements with the temperature we should expect a voltage change at the phase transition. The susceptibility is directly proportional to the voltage difference (for a complete calculation see Appendix C):

$$\chi \propto \Delta U \tag{6.1}$$

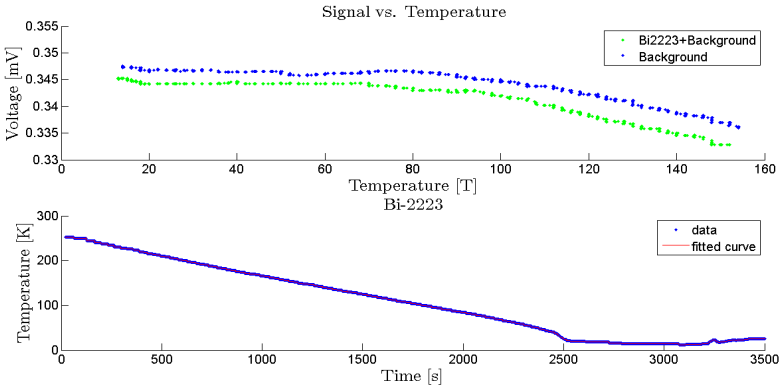

Figure 14: *The temperature vs. signal and the time vs. temperature plots for the Bi-2223 sample.*

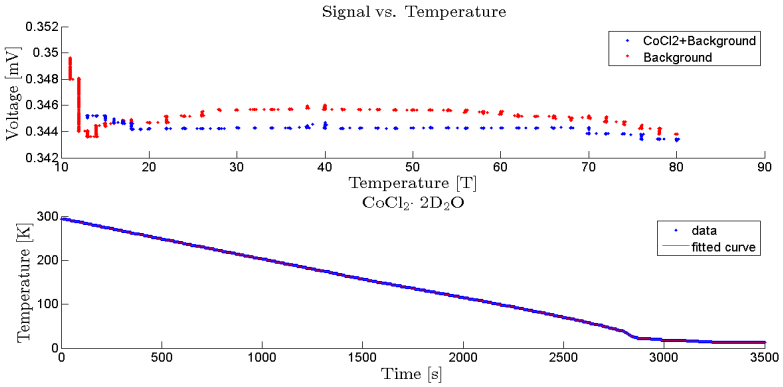

Figure 15: *The temperature vs. signal and the time vs. temperature plots for the $CoCl_2 \cdot 2D_2O$ sample.*

In figure 14 and 15 we show the temperature, time and voltage signals obtained in the experiment. Note that the temperature axes are different. The raw data can be found in Appendix F, figure 25. The data is at first glance ambiguous and no phase transition is obvious. We expected to see a clear phase transition with the Bi-2223 sample at ~ 108 K ([4]), but found no strong deviation from the background signal in that regime. This was quite disappointing to us and has lead us to believe that the setup might have a too low. These considerations will be elaborated further in section 7.

Taking a closer look at the $CoCl_2 \cdot 2D_2O$ data we observe two things. Mainly, the background signal is in general lower than the sample signal which is worrying since we would expect an induced voltage signal from the sample before the phase transition. This makes our data unreliable. Secondly, we do observe some deviation in our sample signal at $\sim$ 17 K which might be promising. From earlier experiments (see section 3) the ordering temperature is found to be 17.5 K [10]. In figure 16 we zoomed in on the data in the region where we expect to find the phase transition:

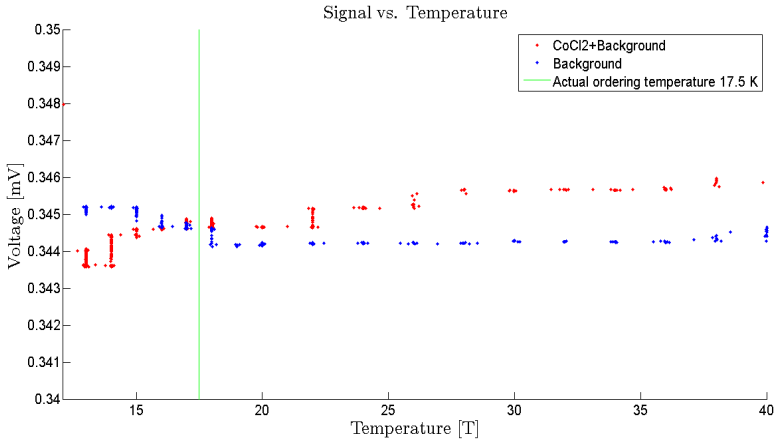

Figure 16: *Voltage signal vs. temperature data for the* $CoCl_2 \cdot 2D_2O$ *sample. We have zoomed in on the region where we expect a phase transition. The ordering temperature is shown as the green line.*

The data clearly show a feature at approximately 17 K. The voltage drops below the background signal which is what we expect to see if a phase transition is present. We were however not able to perform the measurement again since the instrument broke down and we ran out of time. We will discuss this further in section 7.

6.2 FLEXX

In this section we will analyze our measurements on $CoCl_2 \cdot 2D_2O$ when using the FLEXX instrument. Besides measuring at FLEXX, we simulated data using `McStas` to verify our results and calculate the instruments signal resolution.

6.2.1 McStas Simulations

Along with the actual experiment performed at BENSC, a Monte Carlo ray-tracing simulation of FLEXX was used as well to cross check the data obtained.
An instrument file was written in `McStas` ([17]), containing the appropriate instrument settings and crystal properties. From this, simulated elastic incoherent data was created and the resolution of the instrument was calculated through correlation analysis, [16] :

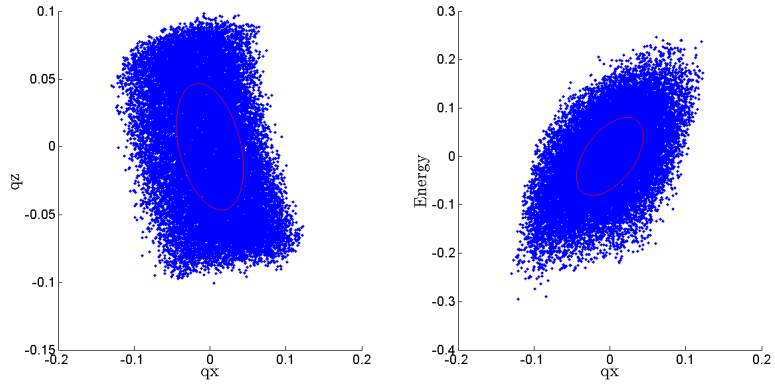

Figure 17: *The resolution ellipsoids for (from left to right): (qx,qz),(qx,energy). All other parameters showed no significant correlation, the rest is shown in Appendix G.*

Using the simulated data, the variance, covariance and standard deviation σ was calculated:

Table 2: `McStas`

Variable	Variance	σ	Covariance
qx [Å^{-}1]	0.0015	0.0387	-
qy [Å^{-}1]	0.0093	0.0964	-
qz [Å^{-}1]	0.0022	0.0469	-
Energy [meV]	0.0064	0.0800	-
qx,qy	-	-	≈ 0
qx,qz	-	-	-7.608 $\cdot 10^{-4}$
qz,qy	-	-	≈ 0
En,qx	-	-	0.0015
En,qy	-	-	≈ 0
En,qz	-	-	-1.999 $\cdot 10^{-4}$

The only significant covariance was found between the engery and *qx*. To calculate the energy resolution of FLEXX we used the variance of the energy, assuming a gaussian energy distribution with a mean zero we find:

$$E_{res} = FWHM = 2.35 \cdot \sigma_E = 0.19meV \tag{6.2}$$

This resolution determines the FWHM of the elastic incoherent signal. If the spin wave excitation is lower than 0.19 meV we will not be able to see it.

6.2.2 FLEXX Measurements

To perform this experiment we had to direct the magnetic field perpendicular to the spins, the b-axis. Due to the monoclinic unit cell of the crystal it was necessary to tilt the crystal by 53.89° with respect to the a-axis, [3], to fulfil these conditions. The crystal was of the size approximately $0.3 \times 0.3 \times 0.5$ cm^3 and surrounded by glue (Araldit 2 component) to hold it in place.
To study the QPT, see figure 4, we used the following magnetic fields: 15.50T, 15.75T, 16.00T, 16.50T and 17.00T. To get the best signal we tried using a fairly large crystal sample that we would align ourselves. However, the sample did not work, forcing us to use a smaller, pre-aligned sample.

Spin waves can be difficult to measure due to the inelastic background signal. Thus, to identify the spin waves the background is measured, fitted and subtracted. The background was measured with elastic neutron scattering, at all applied field values and the data was compared and combined into one dataset, see Appendix E.
The combined background data was removed from the inelastic signal to unveil a clear image of the spin wave. The background was fitted with a Gauss + Voigt function, see figure 18.

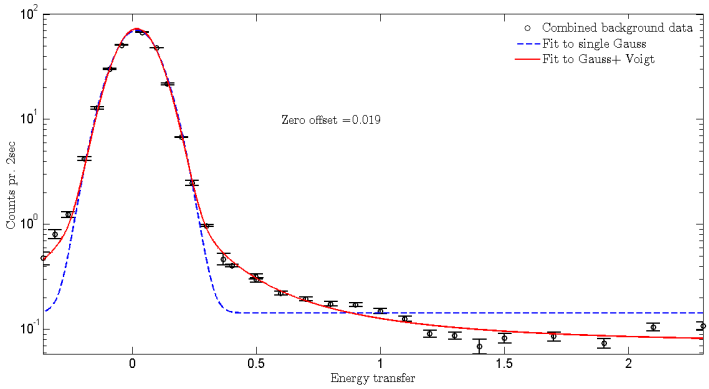

Figure 18: *An illustration of the background data. The blue dotted line indicates the Gaussian fit and the red line indicates the Gaussian + Voigt fit which gives a suitable fit to our data. The FWHM of the background is 0.19*

In table 3 we have listed the FWHM$_E$ and σ_E for both the FLEXX measurement and the `McStas` simulation. They coincide, suggesting that the values lie within the right regime.

Table 3: `McStas` and FLEXX

	FLEXX	`McStas`
σ_E	0.0808	0.0797
FWHM$_E$	0.1903	0.1873

The spin wave signal itself was fitted with a Gaussian function. The clear spin wave image for all applied magnetic fields is shown in figure 19. The figure clearly shows spin waves

appearing when applying an external field. At 16.00 T the spin wave disappears due to the resolution of the instrument, see eq. 6.2, and the tails of the background.

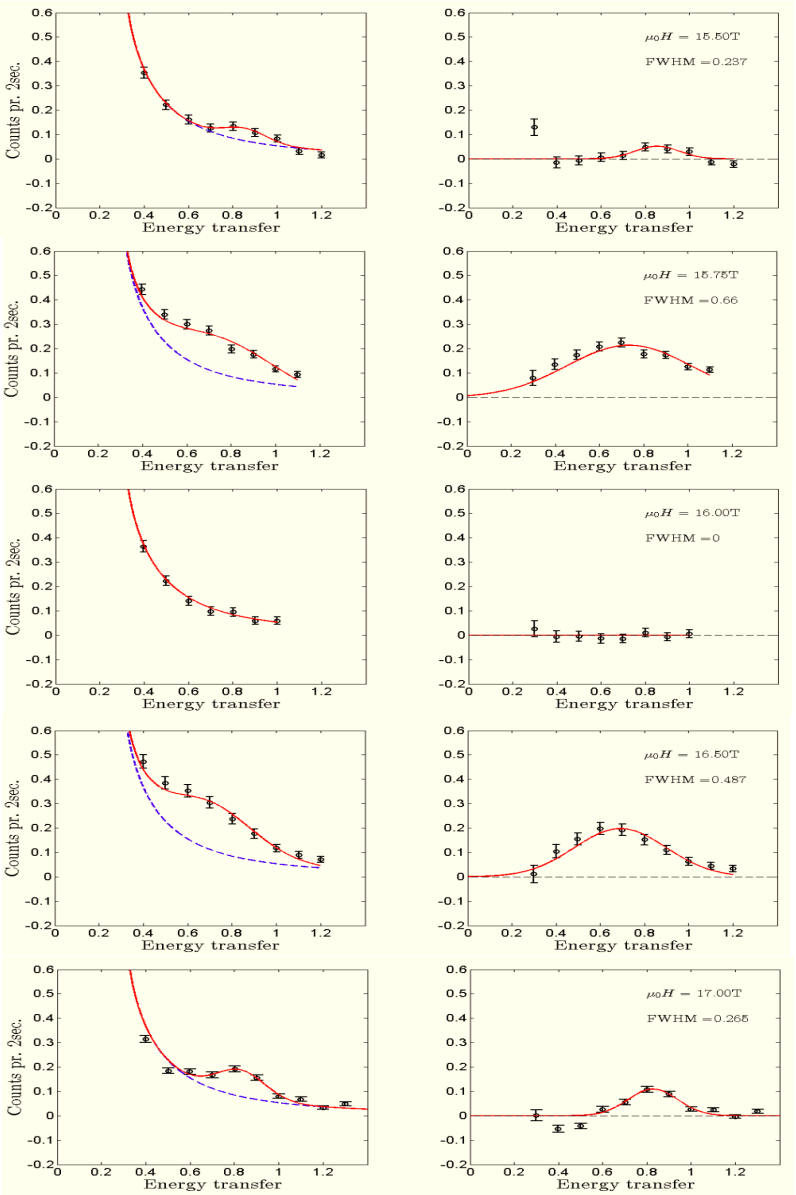

Figure 19: *The **left** images show the Gaussian + Voigt fit to the background and spin wave. The blue dotted line is the fit to the Background and the red line is the fit to the spin wave which contains two Gaussian functions, one for the elastic signal and one for the inelastic signal. The **right** images show just the spin wave and its fit.*

To study the QCP we identify the mean value of the transferred energy at each field and plot the transferred energy as a function of magnetic field strength. Two straight lines are fitted, so the intersection point is the QCP for our measurements, see figure 20.

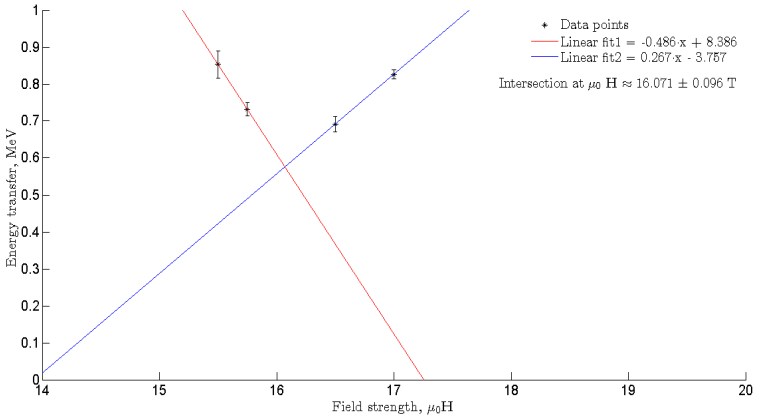

Figure 20: *The energy transfer of the spinewave as a function of the field strength. We fittet two straight lines. Their interception should be the QCP, figure 4. We were not able to measure the actual QCP due to the instruments solution.*

The two straight lines intersects at $\mu_0\mathbf{H} \approx 16.10 \pm 0.10$T, which is close to the expected QCP, which was $\mu_0 H_c = 16.2 \pm 0.05$T, [12]. They agree within one errorbar.
The disappearance of the spin wave at the 16 T field is due to the background tails covering the signal. These tails could not be simulated in McStas fordi spørg kim

7 Discussion

7.1 AC measurements

We have succeed to fabricate an AC susceptometer at which we measured the susceptibility for the superconductor, Bi-2223 and for the $CoCl_2{\cdot}2D_2O$ crystal.
We could not identify a clear phase transition for the Bi-2223 measurements. But there seems to be an indication of a phase transition in the area 80-90 K (figure 14). The signal drops around 80-90 K, then increase and get constant as the background signal.
A way to get a clearer signal may lie in the samples geometry. The intrinsic susceptibility of the Bi-2223 is not quite what we measure experimentally. What we actually measures is [3],

$$\chi_{experiment} = \frac{\chi_{intrinsic}}{1 + N\chi_{intrinsic}}, \tag{7.1}$$

where N is the demagnetization factor and is determined by the geometry of the crystal. For a ferromagnet approaching the Curie temperature, $\chi_{intrinsic} \to \infty$ and $\chi_{experiment} \to 1/N$. Thus, it only depends on the geometry of the material.
Thereby, if the sample was a one piece rod and was larger in size we may have experienced a clearer signal.

The difference in the number of windings has also contributed to the poor quality of the signal. Had the number of windings been the same, it would have bene possible to acheive better sensitivity.

In the $CoCl_2 \cdot 2D_2O$ measurements the background is in general higher than the actual sample signal (figure 15). A possible explanation could be the impurity of the copper wire used for thermal conductivity had some kind of influence on the signal. To prevent this pure silver can be used. This was not available at the time for us, but can be bought home for future prospects.
Further we see some kind of anomaly around 17 K (figure 16) which could be a phase transition, but to establish this as phase transition we need to collect more data and optimize the AC susceptometer.
One optimization could be to ensure the amount of free copper wires which surrounds the cooling finger. The free wires is hard to control and when placing the the shielding cylinder the wires can break or short circuit if it gets in contact with the aluminium case. We experienced short circuit twice, which indicate some electric contact might have been present.

We experienced some problems with the temperature controller. We had some calibrations issues which may not be corrected correctly because of the experiments took place under a vacation week, so the person who had the knowledge was missig. Through luck we managed to get the temperature controller to work, but we are not entirely sure of quality of the outcome.
To make the data collecting and analysing faster, a proper connection between the LakeShore temperature controller and the `LabView` must be done. We did not succeed to do the connect and was forced to use interpolated temperature based on the time and signal which took time and was difficult.

7.2 FLEXX measurements

We succeed to find the spin waves and QCP in $CoCl_2 \cdot 2D_2O$. The experiment had some technical issues, (1) At one particular angle, the analyser arm got stuck, and we had to move it about manually. To prevent this, the floor under the instrument has to be even so for example the analyzer can move freely. (2) One time the monochromator shield was stuck, cause by some thick wires. (3) When doing this experiment the aluminium arm, which connected the sample holder and the detector, was dragged across the floor causing small bending in the arm resulting the detector to be out of alignment.

Even though these technical difficulties was time demanding and could be prevented, it did not have any impact on our data and thereby our analysis of it.
We see a spin wave disappear at 16 T, but we found the solution in the resolution of the instrument and the non-gaussian tails in the background.

To optimize the experiment we could use a larger size crystal and thereby use less glue in the sample holder. Another way to reduce the amount of glue is to mix it with aluminium powder. We need to cover the entire crystal in some kind of substance else it will become spaghetti like, see figure 21.

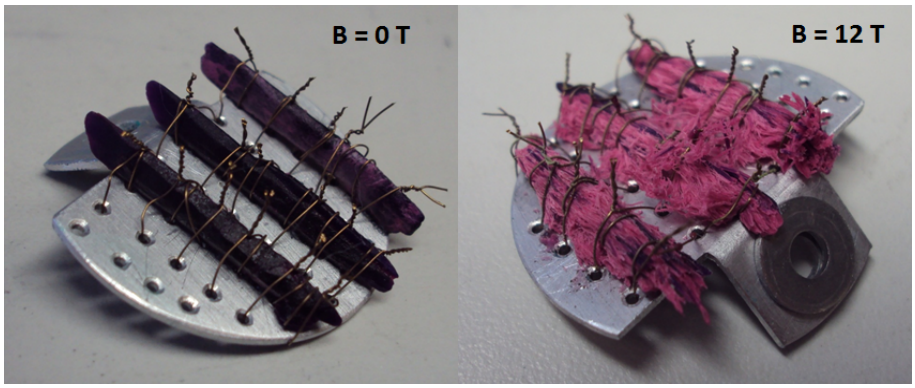

Figure 21: *Three Cobalt crystals used in the time-of-flight spectrometer experiment at SNS at Oak Ridge National laboratory.* ***Left:*** *The crystals before the experiment is performed.* ***Right:*** *The crystals after been exposed to a magnetic field of 12 T.*

8 Conclusion

We were able to get a good measurement of the QCP, despite the possible disappearance of the spin wave at 16 T due to the resolution of FLEXX and the tails of the background. Our result, 16.1 ± 0.1 T not in agreement with 16.2 ± 0.05 T. This is a great success since this is one of the first experiments to measure QPT in a 1D Ising chain.

In the time limit of this bachelor project we succeeded to build a AC susceptometer and we see some promising behaviour around 17.5 K which could indicate a phase transition. This indicates that the idea behind the setup actually works, and given more time and fine adjustment of the coils the possibility of measuring the phase transition is still present.

9 Future Prospects

9.1 AC

If possible, it would be preferred to use a larger setup with the AC-susceptibility measurements. The very thin wires snapped easily making the fabrication extremely slow and difficult. Furthermore, continuous temperature measurements will make the data processing a lot faster and easier along with more reliability. The usage of silver as a thermal conductor and as solder may remove some background fluctuations.
Lastly, but surely important, the two pickup coils must be of the same number of windings to ensure perfect cancellation.

9.2 FLEXX

Regarding the spin wave measurements a larger sample is an obvious improvement. The reduce of glue needed in the sample holder, for example by thinned it with aluminium powder will may remove some of the background noise.
It would be highly interesting to explore the spin waves using a Time of Flight neutron scattering instrument. This allows for the spin wave dispersion, eq. 2.9, to be studied.

References

References

[1] Kim Lefmann "Magnetic Neutron Scattering", Niels Borh Institute 2011

[2] Jacob Larsen, Master Thesis "Quantum phase transition of the near-Ising antiferromagnet $CoCl_2 \cdot 2H_2O$", University of Copenhagen, 2009

[3] Stephen Blundell "Magnetism in Condensed Matter", Oxford University press inc. New York 2007

[4] Webpage "www.wikipedia.org"

[5] Charles Kittel "Introduction to Solid State Physics, eighth edition",eighth edition, Jon Wiley and Sons, Inc 2005

[6] Webpage www.substech.com

[7] J.B. Torrance, Jr and M. Tinkham "Excitation of Multiple-Magnon Bound States in $CoCl_2 \cdot 2H_2O$",Hvarvard University Cambridge Massachusetts, volume 182 no. 2, p. 595, 1969

[8] D. E. Cox, B. C. Frazer and G. Shirane The Magnetic Structure of $CoCl_2 \cdot 2H_2O$, Brookhaven National Laboratories, volume 17 no.2, p.103 - 104, 1965

[9] B. Morosin and Edward J. Graeber A reinvestigation of the crystal structure of $CoCl_2 \cdot 2H_2O$, Sandia Corporation, Albuquerque, New Mexico, p.1176 - 178, 1963

[10] Albert Narath Antiferromagnetism in $CoCl_2 \cdot 2H_2O$.I. Magnetic Structure, Sandia Corporation, Albuquerque, New Mexico, Volume 136 no. 3A, p. A766 - A771, 1964

[11] Sachdev 2001 Quantum Phase Transition

[12] H. Mollymoto, M. Motokawa and M. Date High Field Transverse Magnetization of Ising Antiferromagnet $CoCl_2 \cdot 2H_2O$, Department of Physics, Faculty of Science, Osaka University, Toyonaka, Osaka 560, Volume 49 no. 1, p. 108 - 114, 1980

[13] Griffiths, D. J, 3rd edition Introduction to Electrodynamics, Pearson Education, Inc, 2008

[14] Turi Kirstine Schäffer and Simon Loftager Bachelor Project in Experimental Physics and Crystallization Chemistry, University of Copenhagen, 2010

[15] W. Montfrooij Spin dynamics of the quasi-one-dimensional ferromagnet $CoCl_2 \cdot 2D_2O$, Oakridge National Laboratory, Volume 64, p.134426-1 - 134426-7, 2001

[16] R.J. Barlow Statistics - A Guide to the Use of Statistical Methods in the Physical Sciences, The Manchester Physics Series, John Wiley & Sons, Inc, 1989

[17] Codes used in this project can be found on:
https://www.dropbox.com/sh/obazthww2w89751/g1szWfN1EA

[18] AC Susceptibility Measurements in High-T_c Superconductors, University of Florida

[19] www.mcstas.org

A

Consider the Hamiltonian for the one dimensional $S = 1/2$ Ising model,

$$H = -J \sum_{i}^{N} \mathbf{S}_i^z \cdot \mathbf{S}_{i+1}^z \tag{A.1}$$

for a chain of N spins with periodic boundary conditions, i.e the $S_{N+1}^z = S_1^z$. If $J > 0$ the interaction between the spin favours ferromagnetism.
The energy for a ferromagnetic chain, $|\uparrow\uparrow\uparrow\uparrow\rangle$, is given,

$$E_0 = \langle H \rangle = NS^2 J \tag{A.2}$$

When adding a flipped spin to the chain at the site j, $(1 \leq j \leq N)$, the energy will be,

$$E_1 = -\frac{J}{2} \Bigg[\underbrace{\underbrace{S^2}_{S_1^z S_2^z} + \underbrace{S^2}_{S_2^z S_3^z} + ... + \underbrace{S^2}_{S_{j-2}^z S_{j-1}^z} - \underbrace{S^2}_{S_{j-1}^z S_j^z} - \underbrace{S^2}_{S_j^z S_{j+1}^z} + \underbrace{S^2}_{S_{j+1}^z S_{j+2}^z} + ... + \underbrace{S^2}_{S_N^z S_1^z}}_{1...N} \Bigg] \tag{A.3}$$

$$= -JS^2(N-2) + 2JS^2. \tag{A.4}$$

The costs of energy when flipping a spin will thereby be,

$$\Delta E = E_{cost} = E_1 - E_0 = \underline{\underline{4JS^2}}. \tag{A.5}$$

B

A linear crystal is made up of atoms arranged in a periodic lattice. A lattice is spanned by its basis, a cell that is repeated throughout the entire crystal lattice and connects the atoms in the crystal. In order to describe the position of the atom in the basis, a vector $\mathbf{r}_j$ is defined

$$\mathbf{r}_j = x_j \mathbf{a}_1 + y_j \mathbf{a}_2 + z_j \mathbf{a}_3, \tag{B.1}$$

with $\mathbf{a}_1, \mathbf{a}_2$ and $\mathbf{a}_3$ being the lattice vectors, in the basis, [5]. From eq. B.1 we can define a translational vector that will be invariant under spatial translation if the lattice is periodic:

$$\mathbf{T} = u_1 \mathbf{a}_1 + u_2 \mathbf{a}_2 + u_3 \mathbf{a}_3 \tag{B.2}$$

Where u_1, u_2 and u_3 are integers and denote the planes in the real crystal.
The reciprocal lattice vectors are defined by:

$$\mathbf{b}_1 = 2\pi \frac{\mathbf{a}_2 \times \mathbf{a}_3}{\mathbf{a}_1 \cdot \mathbf{a}_2 \times \mathbf{a}_3} \quad \mathbf{b}_2 = 2\pi \frac{\mathbf{a}_3 \times \mathbf{a}_1}{\mathbf{a}_2 \cdot \mathbf{a}_3 \times \mathbf{a}_1} \quad \mathbf{b}_3 = 2\pi \frac{\mathbf{a}_1 \times \mathbf{a}_2}{\mathbf{a}_3 \cdot \mathbf{a}_1 \times \mathbf{a}_2}. \tag{B.3}$$

From these $\boldsymbol{\tau}$ is formed by :

$$\boldsymbol{\tau} = h\mathbf{b}_1 + k\mathbf{b}_2 + l\mathbf{b}_3, \tag{B.4}$$

and from the Laue Condition $\mathbf{q} = \boldsymbol{\tau}$ we find Bragg's law for diffraction:

$$|\tau|^2 = |\mathbf{k}_i - \mathbf{k}_f|^2 = |\mathbf{k}_i|^2 + |\mathbf{k}_f|^2 - 2\,|\mathbf{k}_i|\,|\mathbf{k}_f|\cos(2\theta) \tag{B.5}$$

We assume that energy conservation is present, so $\mathbf{k}_i = \mathbf{k}_f = \mathbf{k}$,

$$|\tau|^2 = 4\,|\mathbf{k}|^2 \sin^2(\theta) \tag{B.6}$$

Since the wave vector $\mathbf{k}$ is defined as $\frac{2\pi}{\lambda}\hat{\mathbf{k}}$, the length of $\mathbf{k}$ is $\frac{2\pi}{\lambda}$. Using this we get:

$$|\tau| = \frac{2\pi}{d_{(hkl)}} = 2\frac{2\pi}{\lambda}\sin(\theta) \tag{B.7}$$

with $d_{(hkl)}$ being the lattice spacing. This expression finally reduces to the well known Bragg's law:

$$2d\sin(\theta) = n\lambda \tag{B.8}$$

C

In this section we will give the complete description of calculation χ given the voltage difference.
The general expression for the flux of a magnetic field $\mathbf{B}$ through a loop is given [13],

$$\Phi = \int \mathbf{B}\cdot \mathrm{d}\mathbf{A} \tag{C.1}$$

where in our case it is simply,

$$\Phi = NBA \tag{C.2}$$

where N is the number of windings of the coil and A is its cross section. The induced voltage is then, [18],

$$U(t) = -N\frac{\mathrm{d}\Phi}{\mathrm{dt}} = -NA\frac{\mathrm{dB}}{\mathrm{dt}} \tag{C.3}$$

In the experiment we sent the AC signal through the primary coils which produced a voltage output in the pickup coils.
The magnetic field from both the primary coil and the sample coil is denoted $\mathrm{B}_1(\mathrm{t})$ and the resulting magnetic field, from the set of coils without the sample is denoted $\mathrm{B}_2(\mathrm{t})$, which is given,

$$\mathrm{B}_1(\mathrm{t}) \simeq -\mu_0(1 - F\chi)\mathrm{H}(\mathrm{t}) \tag{C.4}$$

and since the applied field is small we can assume,

$$\mathrm{B}_2(\mathrm{t}) \simeq -\mu_0\mathrm{H}(\mathrm{t}) \tag{C.5}$$

where $\mathrm{H(t)} = \mathrm{H}_0 \cos(\omega t)$ is the time-dependent magnetic field generated from the coils, F is the filling factor which is due to the fact that not all of the upper pickup coil's volume is filled with the sample. In general $0 < F < 1$, with $F \simeq 1$ being the case of total fill-out by the sample.
The difference in voltage between the two sets of coils can be calculated to,

$$U^1(t) - U^2(t) = -N_p A_p \frac{\mathrm{dB}_1}{\mathrm{dt}} - \left(-N_p A_p \frac{\mathrm{dB}_2}{\mathrm{dt}}\right) \tag{C.6}$$

$$= N_p A_p \left[-\mu_0(1 - F\chi)\frac{\mathrm{dH}}{\mathrm{dt}} - \left(-\mu_0 \frac{\mathrm{dH}}{\mathrm{dt}}\right)\right] \tag{C.7}$$

$$= -N_p A_p F \mu_0 \chi \frac{\mathrm{dH}}{\mathrm{dt}} \tag{C.8}$$

$$= -N_p A_p F \mu_0 \chi \mathrm{H}_0 \omega \sin(\omega t) \tag{C.9}$$

where N_p is the number of windings for each pickup coil and A_p is its cross section for each pickup coil and H_0 is the amplitude of the applied field for which we will calculate later on.
Since the voltage in each coil oscillates sinusoidally with an angular frequency ω and the amplitude U_0, the voltage difference is also known to be,

$$U^1(t) - U^2(t) = \left(U_0^1 - U_0^2\right) \sin(\omega t) \tag{C.10}$$

By comparing eq. C.9 and eq. C.10 we get;

$$\Delta U = N_p A_p F \mu_0 \chi H_0 \omega \tag{C.11}$$

To a good degree of accuracy we can treat the coils as if they were infinite, in which case the magnetic field is given by,

$$B(t) \approx \frac{N_d \mu_0}{L} I(t) \tag{C.12}$$

where N_d is the number of windings in the primary coil, also called drive coil. Since the magnetic field B(t) and the current I(t) oscillate with the same angular frequency ω, we have that

$$B_0 \sin \omega t \approx \frac{N_d \mu_0}{L} I_0 \sin \omega t \tag{C.13}$$

where B_0 is the amplitude of the magnetic field and I_0 is the amplitude of the current.The sinusoidal behaviour cancels on both sides, leaving us with the relation between the field amplitude and the current amplitude,

$$B_0 \approx \frac{N_d \mu_0}{L} I_0 \tag{C.14}$$

The magnetic field is assumed to be small, so we can approximate it to be $B_0 \approx \mu_0 H_0$, and by comparing it with eq. C.14, we see that the applied magnetic field is

$$H_0 \approx \frac{N_d I_0}{L} \tag{C.15}$$

When using eq. C.15 and eq. C.11 we can find the susceptibility χ to be,

$$\chi = \frac{L}{N_d N_p A_p F \omega \mu_0 I_0} \Delta U \tag{C.16}$$

This equation give us the ability to find the magnetic susceptibility for our system when measuring the voltage difference.

D

The study of linear relation between the ingoing and outgoing voltages signal at room temperature. To study the relationship in the voltage frequency the amplitude was hold at the same value and vice versa. The collected data at room temperature and pressure is presented in table 4 and table 5 and in the figure 22 and 23.

$\boldsymbol{\nu}_{in}$ [Hz]	$\mathbf{I}_{out}$ [mV]	**Phase** [◦]
100,34	0,00	0,00
150,00	0,20	-66,04
200,00	0,27	-74,25
250,00	0,33	-78,46
300,00	0,40	-80,54
350,00	0,47	-81,88
400,00	0,53	-82,88
450,00	0,60	-84,35
500,00	0,67	-84,91
550,00	0,73	-85,36
600,00	0,80	-86,22
650,00	0,88	-86,53
700,00	0,95	-87,18
750,00	1,01	-87,74
800,00	1,08	-88,24
850,00	1,15	-88,67
900,00	1,21	-89,06
950,00	1,28	-89,41
1000,00	1,36	-89,72

Table 4: *The measured amplitude out of the system and the phase difference between the two sets of coils in steps of 50 Hz. The amplitude of the voltage into the system was kept at 1.V.*

$\mathbf{I}_{in}$ [V]	$\mathbf{I}_{out}$ [mV]	**Phase** [◦]
10,6	0,81	-90,00
0,7	0,95	-90,00
0,8	1,08	-90,00
0,9	1,21	-90,00
1,1	1,36	-89,72
1,1	1,49	-89,74
1,2	1,63	-89,77
1,3	1,76	-89,78
1,4	1,90	-89,80
1,5	2,03	-89,81
1,6	2,17	-89,83
1,7	2,30	-89,84
1,8	2,43	-89,84
1,9	2,58	-89,85
2,0	2,71	-89,86
2,1	2,85	-89,87
2,2	2,98	-89,88
2,3	3,11	-89,88
2,4	3,25	-89,89

Table 5: *The measured amplitude out of the system and the phase difference between the two sets of coils in steps of 0.1V. The frequency of the voltage into the system was kept at 245.9 Hz.*

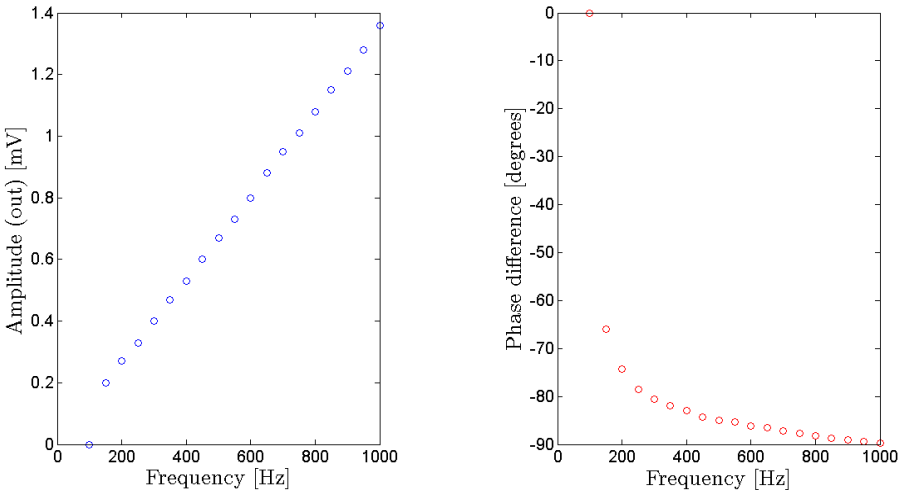

Figure 22: ***Left**: The voltage amplitude (out) as a function of the frequency. **Right**: The phase difference between the two sets of coils as a function of the frequency.*

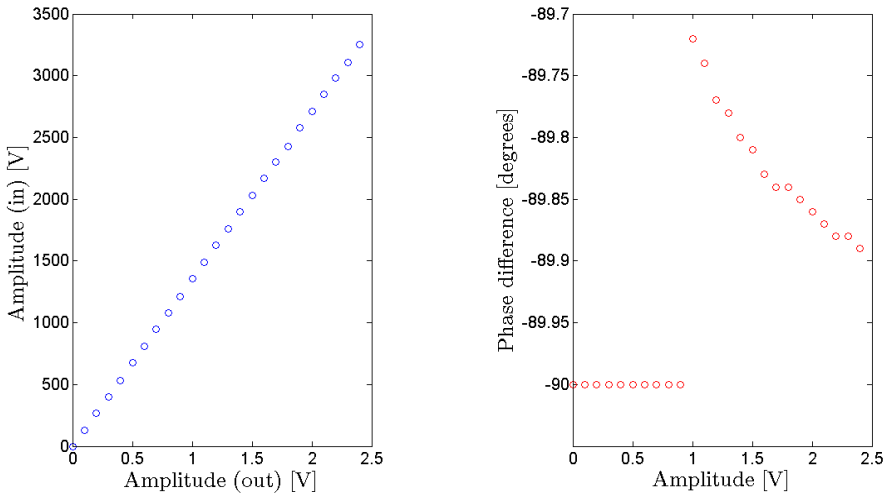

Figure 23: ***Left**: The voltage amplitude (out) as a function of the voltage amplitude (in). **Right**: The phase difference between the two sets of coils as a function of the voltage amplitude (in).*

E

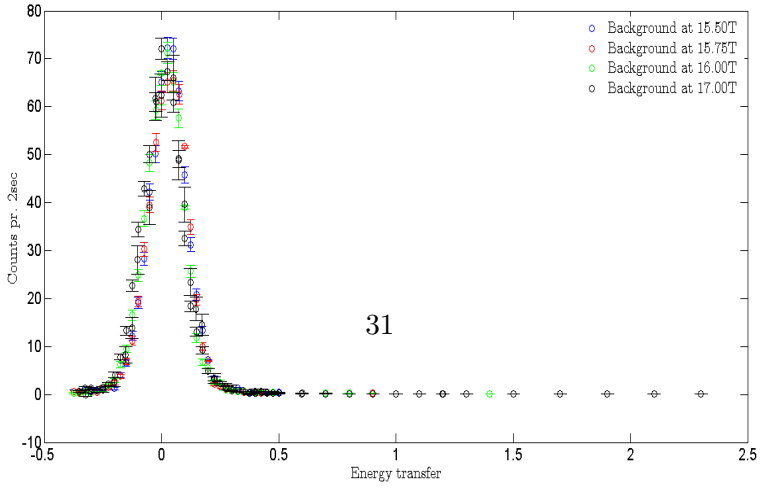

F

Susceptometer raw data:

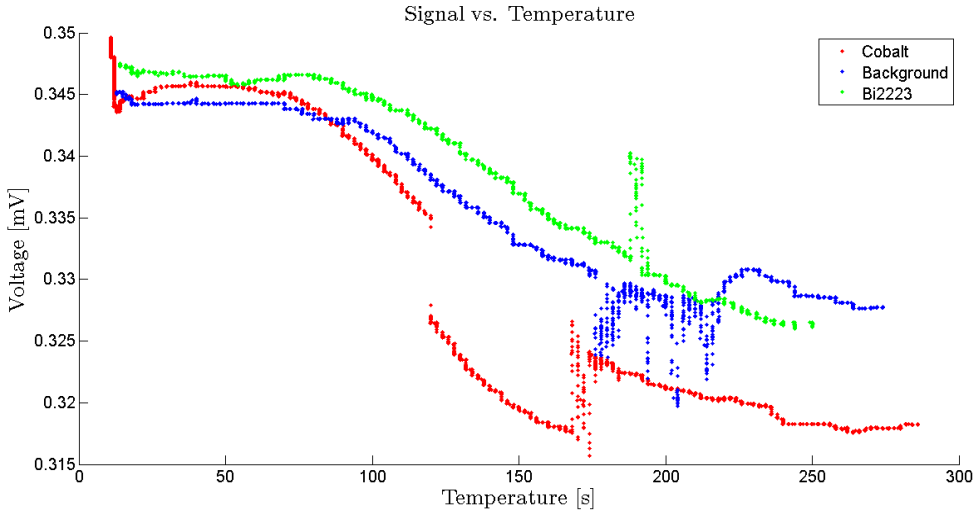

Figure 25: *The background, Bi-2223 and $CoCl_2 \cdot 2D_2O$ signal plottet as a function of temperature. Red is $CoCl_2 \cdot 2D_2O$, blue is the backround measured with the copper wire and bee wax still in the sample holder, and green is the superconductor sample Bi-2223.*

Figure 25 shows the raw data from the susceptibility experiment. Due to the amount of noise in the high temperature range, we chose to cut the data to include 150 K - 11 K and discard the rest. We expect to see a phase transition at $\sim$ 108 K for the superconductor and $\sim$ 17 K for $CoCl_2 \cdot 2D_2O$. The data however is not pleasant to work with due to noise, and the fact that the background signal is lower than the actual sample signal i worrying.

As presented in the project we do find some deviation from the background signal with the $CoCl_2 \cdot 2D_2O$ sample at $\sim$ 17 K which might originate from a phase transition. The Bi-2223 sample did not show any distinctive behaviour. This might originate from the size of the sample that was remarkably smaller than the $CoCl_2 \cdot 2D_2O$ crystal used.

G

Correlation ellipsoids

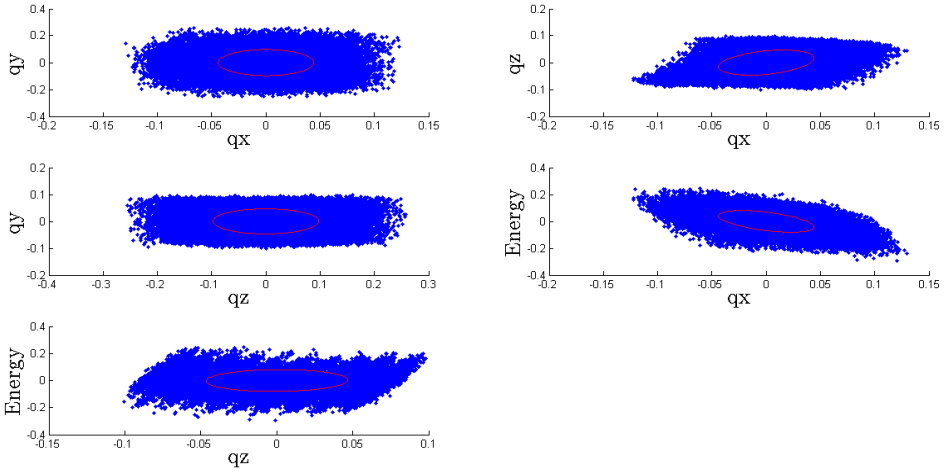

Figure 26: *The resolution ellipsoids for (from left to right): (qx,qy), (qx,qz), (qz,qy), (qx,energy), (qz,energy). (qx,qy) and (qz,qy) seem relatively uncorrelated, whereas the rest show correlation.*